IPSJ Transactions on Computer Vision and Applications Vol.6 34–38 (July 2014)

[DOI: 10.2197/ipsjtcva.6.34]

Express Paper

Polarimetric Endoscope for Image Enhancement of Surface Micro-structure on Mucosa

Katsuhiro Kanamori[1,a)]

Received: March 14, 2014, Accepted: April 24, 2014, Released: July 25, 2014

Abstract: This paper presents a novel image processing method to enhance appearance of micro-structure of a living-organ mucosa using polarized lighting and imaging. A new technique that uses two pairs of parallel and crossed nicol polarimetric images captured under two different linearly polarized lightings are presented, and an averaged subtracted polarization image (AVSPI) which is calculated from the above four images is introduced. Feasibility experiments were performed using the prototype of polarimetric endoscope hardware using excised porcine stomachs.

Keywords: polarization, image enhancement, translucent object, grooves, mucosa, endoscope

1. Introduction

In the field of an endoscopic inspection of an early stage of gastric or colon cancer, the close inspection of the micro-structure on mucosa surface is important. However, it is difficult to observe the micro-structure under the ordinary non-polarized white light due to its translucent optical characteristics, and invasive methods such as spraying indigocarmine blue fluid have been used. The objective of this study is to develop a novel endoscope that can observe the micro-structure of mucosa surface clearly using non-invasive polarimetric imaging. Various polarization techniques have been studied in the field of dermatlogy [1], [2], [3], endoscopy [4], or pathological diagnosis [5], [6], but there is no mention of the above subject. The subtracted polarization technique that has been used for the separation between the superficial and the deeper layer information of translucent medium is newly applied for the contrast enhancement of surface micro-structure.

In this paper, Section 2 explains the theoretical background for the detection of the groove region on the translucent medium by using polarization image capturing. Section 3 presents a new technique that uses two pairs of parallel and crossed nicol polarimetric images and an averaged subtracted polarization image (AVSPI) is introduced. Image processing flow for the enhancement of the micro-structure is also explained. Section 4 presents the prototype of the polarimetric endoscope hardware and shows the results from the experiments using gastric mucosa samples from excised procine stomachs. Section 5 concludes this work.

2. Theoretical Background

2.1 Backscattering of Polarized Light Near the Surface Layer of Mucosa

Figure 1 (a) shows the schematic intersection that linearly polarized light enters into the surface mucosa of organ from vertical upper part. The surface micro-structure is modeled as simple grooves that run in a direction perpendicular to the paper surface. Here, the reflected lights that returns to the camera can be divided into the following three types.

- Specular reflected light, or halation that maintains the incident polarization state [SR].
- Backscattered light from the superficial layer of mucosa that maintains the incident polarization state [SR1].
- Backscattered light from the surface that once penetrated to the deeper layer of mucosa and de-polarized by the multi-scattering [D], [DR].

Here, [DR] polarizes again when it is emitted from the groove in the direction perpendicular to groove direction by the diffuse polarization phenomenon [7], [8], [9]. Figure 1 (b) shows the relationship of the emittance angle and the degree of polarization in the diffuse polarization phenomenon derived from Fresnel theory of reflection. In case of biological tissues that have the refractive index around 1.33 has the degree of polarization (DOP)=0.05 under the condition of emittance angle of 45° ∼ 60°.

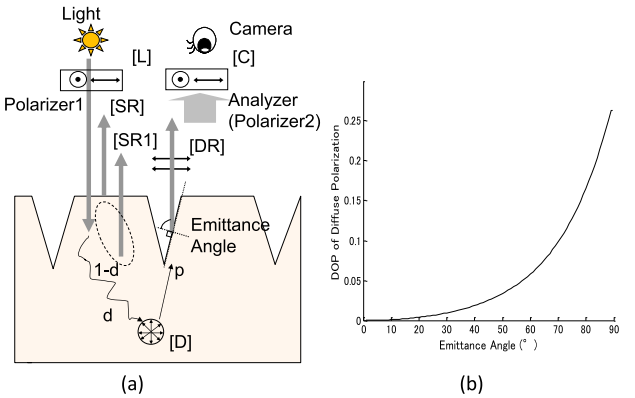

Fig. 1 Principle of polarimetric imaging (a) Model of intersection of mucosa and polarimetric measurement (b) Degree of polarization (DOP) by the diffuse polarization at groove region.

[1] Advanced Technology Research Laboratories, Panasonic Corporation, Kyoto 619–0237, Japan
[a)] kanamori.katsuhiro@jp.panasonic.com

2.2 Contrast Enhancement of Grooves Using Polarized Light

Figure 2 explains the observed intensity in case the incident light enters into the surface groove and the plane region from vertical upper part and returns back to the camera neglecting the light absorption effect [10]. We assume the groove axis is 45° to the polarization axis of incident light 0° or L0 because the surface of biological tissue is optically incomplete and its direction can be modeled as random. Two different polarization status of cameras are denoted as C0 and C90, which means polarized axis is 0° and 90°. The combination of light and camera polarization status is expressed as L0C0 or L0C90.

In case that the polarized light enters into the groove region, as shown in Fig. 2 (a), L0 can be divided into L45 and L135 with the equal power of 1/2. Using the Malus' law and the fact that the linear polarizer transmits only 1/2 of de-polarized light, the intensity $I[L0C0](\|)$ and $I[L0C90](\perp)$ are given as the following.

$$\begin{aligned} I[L0C0] &= I[L0C90] \\ &= 1/2 \times [\cos^2 45^\circ \times (d_1 p + (1 - d_1) + d_2 p \\ &+ (1 - d_2)) + 1/2 \times d_1(1 - p) + 1/2 \times d_2(1 - p)] \\ &= 1/2. \end{aligned} \tag{1}$$

Here, the intensity of input light is assumed to be 1 and d_1 and d_2 $(0 < d_1, d_2 < 1)$ denote de-polarized ratio of the input polarized light for L45 and L135 case respectively and p denotes the diffuse polarized ratio shown in Fig. 1 (b). This result shows that $I[L0C0]$ and $I[L0C90]$ are the same at the groove region, and the subtracted polarization image$(I[L0C0] - I[L0C90])$ is nearly zero, which means the groove region looks very dark with this polarimetric imaging.

In case of the polarized light enters into the plane region, as shown in Fig. 2 (b), the intensity in the parallel nicol and crossed nicol are given using de-polarized ratio $d(0 < d < 1)$ by the following equations respectively.

$$(I[L0C0] = 1 - d/2) > (I[L0C90] = d/2). \tag{2}$$

This result shows the subtracted polarization image $(I[L0C0] - I[L0C90])$ at the plane region always looks light with this polarimetric imaging. As a result, the subtracted polarization image has a pretty high (theoretically ∞) contrast between the groove and the plane regions.

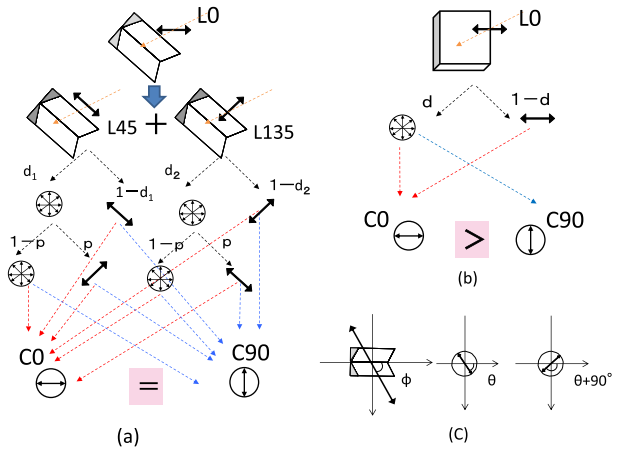

Fig. 2 Polarized light observed by parallel and crossed nicol states (a) Groove region, (b) plane region, (c) Angle of groove ϕ and angle of polarized observation θ for the non-polarized measurement calculation.

2.3 Contrast Enhancement of Grooves Using Non-polarized Light

The intensity contrast of using non-polarized light is investigated. The calculation is executed under the assumption of the incident non-polarized light is the average of each polarized light power with the polarized plane angle of ϕ and the observed light intensity is the sum of the light power through the analyzer with the angle θ and θ+90°.

In case of the groove region, the intensity of $I(\theta)$ and $I(\theta + 90^\circ)$ are given as

$$\begin{aligned} I(\theta) = 1/\pi \int_0^\pi d\phi [&\cos^2\phi \times [(1 - d_1)\cos^2\theta + d_1 p \sin^2\theta] \\ &+ \sin^2\phi \times [(d_2 p \sin^2\theta + (1 - d_2)\sin^2\theta] \\ &+ \cos^2\phi \times d_1(1 - p)/2 + \sin^2\phi \times d_2(1 - p)/2]. \end{aligned} \tag{3}$$

$$\begin{aligned} I(\theta + 90^\circ) = 1/\pi \int_0^\pi d\phi [&\cos^2\phi \times [(1 - d_1)\sin^2\theta + d_1 p \cos^2\theta] \\ &+ \sin^2\phi \times [d_2 p \cos^2\theta + (1 - d_2)\cos^2\theta] \\ &+ \cos^2\phi \times d_1(1 - p)/2 + \sin^2\phi \times d_2(1 - p)/2]. \end{aligned} \tag{4}$$

The measured intensity is given by adding the above two equations as below.

$$I(\theta) + I(\theta + 90^\circ) = 1. \tag{5}$$

In case of the plane region, the intensity is 1, because all the input power reflects back to the camera under no absorption assumption. These results mean that the observed intensity at the groove region as well as the plane region is the same. Therefore, the contrast between the groove and the plane region is very poor, which is the reason for the invisibility of the surface microstructure under non-polarized white light.

3. Polarimetric Image Processing for Enhancement of Surface Micro-structure

3.1 The Averaged Subtracted Polarization Images

Figure 3 shows an capturing of parallel and crossed polarization image pair and subtraction process. The polarized axes of the linearly polarized light changes by turns, and two pairs of parallel and crossed nicol polarimetric images are captured under each lighting status. Then, parallel nicol (||) and crossed nicol (⊥) pairs

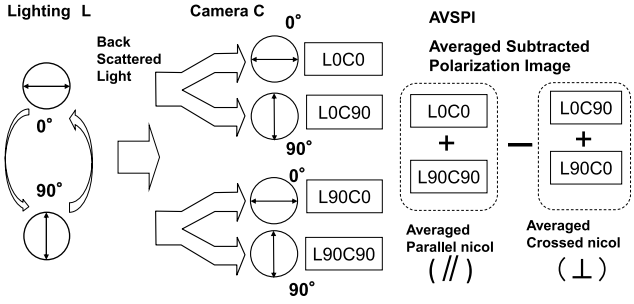

Fig. 3 Averaged subtracted polarization image (AVSPI).

are averaged, subtracted, and an averaged subtracted polarization image (AVSPI) is calculated.

$$\begin{aligned}\mathrm{AVSPI} &= (I[L0C0] + I[L90C90])/2 \\ &\quad - (I[L0C90] + I[L90C0])/2. \end{aligned} \tag{6}$$

AVSPI is used for the subsequent image processing for the groove detection. This new concept is introduced due to two reasons. First, there are some difference of image quality by the difference of polarization direction of the light because of the object surface has slope and anisotropy. Second, the color polarization camera used for the prototype endoscope has two independent optical paths including color image sensors and the illuminance of L0/L90 LED light are not exactly the same, therefore, a simple subtraction process between the two captured images causes poor results. AVSPI can create the same measurement characteristics for the parallel and crossed nicol observation to solve the above problems.

3.2 Image Processing for Groove Detection and Enhancement

Figure 4 shows the overall image processing for the groove detection and color enhancement processing. This image processing uses AVSPI as an input image in case of the polarimetric image processing, and color intensity image in case of the conventional intensity image processing.

At first, low pass filtering (LPF) is executed, then the space differential operation is executed to detect the surface groove regions as the intensity edges. This is executed only for the green component of the color image concerning the green plane image has less image noise, and the penetration of green light into the medium is not so deep. The space differential filter (5×5 pixels) is designed to detect the groove region for four directions, horizontal, vertical, upper right, and lower right. And the maximum intensity difference value between the center and the both ends pixels for the four directions is determined as Δ-Value, and this is output as the result image of the space differential processing.

The blue component enhancement block enhances the blue-color component using calculated Δ-Value. This procedure is executed by leaving the blue component as is and subtracting some constant multiplied Δ-Value from red and green component [11]. This block outputs two images. One is Enhanced Color Intensity Image (1) in which the detected groove region is enhanced by bluish color, and the other is the Groove Gray Image that represents the groove position and edge strength as gray intensity.

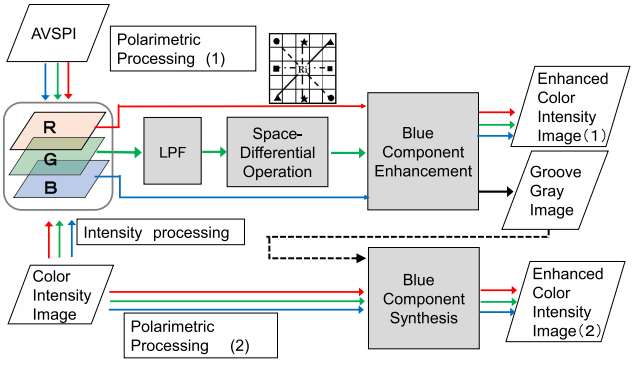

Fig. 4 Image processing for detection and color enhancement of groove regions.

Polarimetric processing (1) can't reproduce the correct mucosa color in case of AVSPI that has lost the correct color, therefore, Polarimetric Processing (2) is used. This processing synthesizes Enhanced Color Intensity Image (2) which is a result of two images syntheses, Color Intensity image and Groove Gray Image together and this image is more suitable for the pseudo indigo-carmine sprayed images.

4. Experimental

4.1 Polarimetric Endoscope Hardware

As shown in **Fig. 5**, the prototype endoscope hardware consists of three parts, a color-polarization camera, a rigid-scope and a LED-polarized light. The FD-1665 3-CCD Camera (FluxData, Inc.) uses 3-way prism beam splitter that splits the incoming white light into three components with equal spectral and three single-chip color CCD image sensor (658×492 pixels and 8/12 bit for R, G and B-channel) which have 0°/45°/90° polarizer on them. The extinction ratio of these polarizers are 3000:1 [12]. The only two (0°/ 90°) CCD are active in this prototype and these two polarization full color images (C0 and C90) are given in real-time and simultaneously.

The rigid scope (MILS SYSTEMS co., ltd ϕ=5.8×135 mm View Angle=40°) doesn't use the original fiber illumination system, and a 35 mm lens is used to interface these two optical systems; the color-polarization camera and the rigid scope.

The specially designed LED-polarized light (ϕ=34 mm) is set at the tip of the rigid scope. This ring-shaped light consists of eight sub-LED lamps with 2-channels (Ch) of four lamps. 1-Ch and 2-Ch have 0° and 90° polarizer on the lamps respectively and can be lit independently by turns to change the polarization axis. Each channel has the illuminance of 5,000 lx at 50 mm distance from the tip. Polarization axis change and image capturing are synchronized using the control software on the host computer. The total extinction ratio of this prototype endoscope is 80:1 to 100:1 from the image contrast measuring of input linearly polarized light.

4.2 Result of Image Processing and Effectiveness of AVSPI

The gastric mucosa samples from porcine stomachs are excised and polarimetric capturing and imaging was conducted using the prototype endoscope. Observation was executed with 50 mm distance from the tip and the observation region was carefully se-

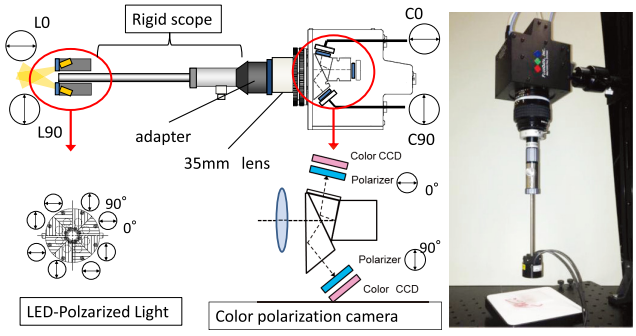

Fig. 5 Prototype polarimetric endoscope.

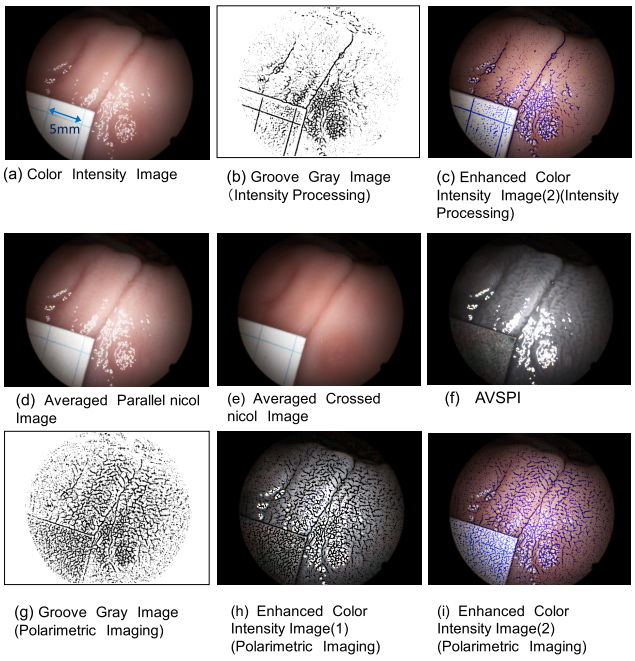

Fig. 6 Captured images of porcine gastric mucosa and results of image processing.

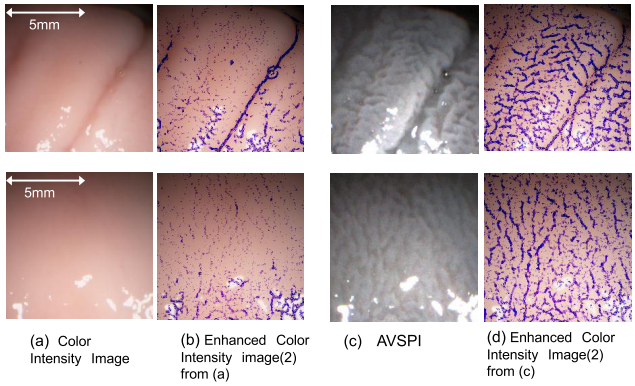

Fig. 7 Enhancement of micro-structure by using conventional color image and polarimetric image (close-up).

lected so as not to include large halation portion.

Figure 6 shows all nine types of processed images that the endoscope can generate online. Figure 6 (a) shows the color intensity image captured by the prototype endoscope under non-polarized lighting with the LED-polarized light all on. Figure 6 (b) and (c) show Groove Gray Image and Enhanced Color Intensity Image (1) by the intensity processing in Fig. 4.

Figure 6 (d) and (e) show the averaged parallel and crossed nicol image that are also captured by the endoscope with the sub-LED-polarized light on by turns. Figure 6 (f) shows AVSPI, and this is nearly gray image, which means the superficial layer of gastric mucosa has no blood vessel and no color. Figure 6 (g)–(i) show Groove Gray Image, and Enhanced Color Intensity Image (1) and (2) by the polarimetric processing (1) and (2) in Fig. 4. Comparing between (b) and (g), or (c) and (i) shows that the polarimetric processing results can enhance more detail information than the conventional intensity processing.

Figure 7 shows the comparison of color images processing and polarimetric processing for the close-up of two different portions. Figure 7 (a) and (b) show Color Intensity Image and Enhanced

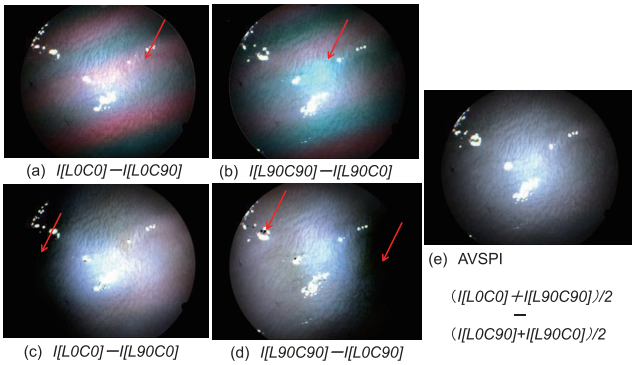

Fig. 8 The effectiveness of AVSPI compared with four types of simple subtraction of polarization images.

Color Intensity Image (2). Figure 7 (c) and (d) show AVSPI and Enhanced Color Intensity Image (2). The micro-structure is nearly invisible in Fig. 7 (a) and (b), even if the image enhancement is done. On the other hand, detailed structure can be seen in Fig. 7 (c) and (d), and these are quite similar to the indigocarmine sprayed image. These results suggest the effectiveness of present polarimetric endoscope.

Figure 8 shows the effectiveness of AVSPI. There are two pairs of parallel and crossed nicol polarimetric images, therefore there are four types of simple subtracted polarization images. They are (a) $I[L0C0] - I[L0C90]$, (b) $I[L90C90] - I[L90C0]$, (c) $I[(L0C0] - I[L90C0]$ and (d) $I[L90C90] - I[L0C90]$. Here, a) and b) have different optical path and use different image sensors, and c) and d) have some difference in polarized lighting status, and these factors cause poor image quality as shown in Fig. 8.

The colored stripe artifacts in Fig. 8 (a) and (b) are caused by a different optical path in the 3-way prism beam splitter and it is difficult to remove these color artifacts completely even if some image calibration procedure is applied. The dark regions and black spots in Fig. 8 (c) and (d) are caused because the crossed nicol image has greater pixel values than the parallel nicol image. Such unexpected phenomenon occurs due to the non-uniformity of the lighting and insufficient halation removing due to relatively low extinction ratio. On the other hand, AVSPI shown in Fig. 8 (e) has no artifacts, and the poor image quality of the simple subtracted polarization images (a)–(d) is completely resolved.

5. Conclusion

A novel polarimetric imaging method for the endoscopy of invisible surface micro-structure on mucosa is presented. Two pairs of parallel and crossed nicol polarimetric images captured under two different linearly polarized lighting are used and an averaged subtracted polarization image (AVSPI) is introduced. The prototype of rigid-type polarimetric endoscope with the extinction ratio over 80:1 is developed, and this system can execute the observation and image processing online. Though this prototype can't be inserted into a living body due to its size problem, it is quite useful for basic investigation using excised samples.

The experiments using a gastric mucosa of porcine were executed, and pseudo indigocarmine sprayed images that enhance the micro-structure were created. These images are better than the result from the conventional color intensity imaging, and this work

suggests the effectiveness of polarimetric endoscope for close inspection of mucosa surface.

References

[1] Smith, M.H., Burke, P., Lompado, A., Tanner, E. and Hillman, L.W.: Mueller matrix imaging polarimetry in dermatology, *Biomedical Diagnostics, Guidance, and Surgical-Assist System II*, *Proc. SPIE*, Vo-Dinh, T., Grundfest, W.S., Benaron, D.A. (Eds), Vol.3911, pp.210–216 (2000).

[2] Jacques, S.L., Ramella-Roman, J.C. and Lee, K.: Imaging skin pathology with polarized light, *Journal of Biomedical Optics*, Vol.7, No.3, pp.329–340 (July 2002).

[3] Ramella-Roman, J.C., Lee, K., Prahl, S.A. and Jacques, S.L.: Polarized light imaging with a handheld camera, *SPIE Vol.5068, Saratov Fall Meeting 2002: Optical Technologies in Biophysics and Medicine IV* (13 Oct. 2003).

[4] Kagawa, K., Shogenji, R., Tanaka, E., Yamada, K. and Kawahito, S.: Variable field-of-view visible and near-infrared polarization compound-eye endoscope, *34th Annual International Conference of IEEE EMBS*, San Diego, California USA, pp.3720–3723 (2012).

[5] Pierangelo, A., Manhas, S., Benali, A., Antonelli, M.-R., Novikova, T., Validire, P., Gryet, B. and De Martino, A.: Use of Mueller polarimetric imaging for the staging of human colon cancer, *Optical Biopsy IX, Proc. SPIE*, Alfano, R.R., Demos, S.G. (Eds.), Vol.7895, 78950E-1–8 (2011).

[6] Novikova, T., Pierangelo, A., De Martino, A., Benali, A. and Validire, P.: Polarimetric Imaging for Cancer Diagnosis and Staging, *OPTICS & PHOTONICS NEWS OCTOBER 2012*, pp.28–33 (2012).

[7] Atkinson, G.A. and Hancock, E.R.: Recovery of surface orientation from diffuse polarization, *IEEE Trans. Image Proc.*, Vol.15, No.6, pp.1653–1664 (2006).

[8] Miyazaki, D. and Ikeuchi, K.: Basic Theory of Polarization and Its applications, *IPSJ Trans. Computer Vision and Applications*, Vol.1, No.1, pp.64–72 (2008). (in Japanese).

[9] Miyazaki, D., Tan, R.T., Hara, K. and Ikeuchi, K.: Polarization-based Inverse Rendering from a Single View, *Proc. International Conference on Computer Vision*, pp.982–987, Nice, France (2003).

[10] Kanamori, K.: Image enhancement of surface micro-structure on mucous membrane by polarized image, *19th Symposium on Sensing via Image Information* (*SSII2013*), IS3-01-1-IS3-01-8 (2013). (in Japanese).

[11] Japanese Patent No.3869698. (in Japanese).

[12] Imaging Polarimeters: A WEB Page, FluxData, Inc. (online), available from ⟨http://www.fluxdata.com/imaging-polarimeters⟩ (accessed 2014-05-12).

(Communicated by *Yoshito Mekada*)